Chalcogenide Letters Vol. 11, No. 1, January 2014, p. 37 - 45

ENHANCED GRAIN GROWTH IN THE Sn DOPED Sb_2S_3 THIN FILM ABSORBER MATERIALS FOR SOLAR CELL APPLICATIONS

B. ISMAIL[a,*], S. MUSHTAQ[b,c], A. KHAN[b]
[a]*Department of Chemistry, COMSATS Institute of Information Technology, Abbottabad 22060, Pakistan*
[b]*Department of Applied Physics, Federal Urdu University of Arts, Science and Technology, Islamabad 44000, Pakistan*
[c]*Nanoscience and Catalysis Division, National Centre for Physics, Quaid-e-Azam University Campus, Islamabad 44000, Pakistan*

The effects of doping of Sn on the structural, morphological, electrical and optical properties of Sb_2S_3 thin films have been investigated. The annealing of thin films at 250 ºC for a time of 2 hrs under vacuum has a marked effect on the properties of the thin films. The diffusion of elements into the glass substrate is observed while the possibility of the oxidation of the thin films is nullified based on the determination of experimental composition by RBS. The average thickness of the thin films was 120 -250 nm. The grain growth is enhanced on the account of doping while uncontrolled growth is observed in the undoped thin film samples. The materials are found to be the direct band materials with the energy band gap values of 1.5-1.9 eV. The values of absorption coefficient range from 0.09-1.11 x 10^5 cm^{-1}. The maximum value of refractive index is 4.20 at 417 nm and annealing under vacuum lowers its value to below 3.8. The dielectric constant has a maximum value of 20 at 525 nm and annealing lowers the dielectric constant values.

(Received October 21, 2013; Accepted January 24, 2014)

Keywords: Chalcogenides, solar cells, absorption coefficient, X-ray diffraction, electrical conductivity, band gap

1. Introduction

Energy shortage and the environmental pollution are the outcomes of continuously increasing population. The sustainable human development will depend upon the alternative energy resources because the availability of the natural reserves of coal, gas and oil is uncertain due to imbalance of demand and supply. Possible alternatives to natural resources include non-conventional oil and gas, nuclear power, wind, tidal, solar, geothermal, hydrogen, etc [1]. Solar energy is a cheap and convenient alternative to natural reserves as earth receives plenty of it every day [2]. One of the ways of utilizing the solar energy is the photovoltaic technology which employs an absorber material that captures the sunlight for the generation of electricity. Currently, the photovoltaic market share is dominated by the crystalline Si (single or multicrystalline) solar panels (> 80%) while the thin film panels (amorphous/micromorph Si, CdTe, copper-indium-selenide/copper-indium- gallium-diselenide CIS/CIGS) contribute < 20% [3]. The most advanced configurations of solar cells include dye sensitized solar cells, quantum dot solar cells, concentrator solar cells, organic/polymer solar cells, etc which are not yet commercialized. The future of solar cell industry relies on two aspects: viz: cost and efficiency. Thin films offer many advantages over single crystals e.g. ease of fabrication, cost effectiveness, small amounts of materials used, etc., and currently thin film solar cells reached the efficiencies of 19 % [4]. The high processing cost of elemental Si, toxicity of Cd, rare existence of Te and In and high

*Corresponding author : bushraismail@ciit.net.pk

operational cost for CIGS manufacturing has boosted research efforts to discover cheap, less toxic, abundant and simple two or three component absorber materials having suitable band gaps for capturing the maximum sunlight [3].

Recently, compounds of group 15-16 have gained attention due to their suitable optical and electrical properties [5]. Among them, amorphous antimony trisulphide chalcogenide (stibnite phase, Sb_2S_3) has been used for different application as in television cameras, microwave devices, switching devices, and optoelectronic devices, etc. In its nano or polycrystalline form, Sb_2S_3 is a good absorber material for photovoltaic applications with a band gap of 1.5-2.8 eV (depending upon the crystallinity) and absorption coefficient of the order of $\sim 10^4$ cm^{-1} and a high refractive index of 2.4-3.2 (depending upon deposition temperature) [6]. Different configurations of solar cell structures employing Sb_2S_3 have been used, for example, Ag/Sb_2S_3:C/CdS/ITO, CdS/Sb_2S_3/PbS, p-Sb_2S_3/n-Si heterojunctions [7], Pt-Sb_2S_3 and n-Sb_2S_3/p-Ge [8] and the conversion efficiencies of up to 7.3 have been reported.

The main focus of the research work on antimony sulphide has been on the deposition and characterization of antimony sulphide thin films. Only recently, the effects of doping of various ions on the properties of Sb_2S_3 have gained attention due to the increased need for the optimization of optical and electrical properties for the appropriate use as an absorber material in solar cell applications. The doping effects of Ag [9], C [10], Cu [11], Mg [12] and Sm [13] are already reported. The extensively studied dopant element for the Sb_2S_3 lattice is Sn as evident from the large number of reports. The crystal structure determination of $SnSb_4S_7$ [14], optical properties of $SnSb_2S_4$ [15] and $SnSb_2S_5$ [16] have been investigated. The optical properties of Sn doped amorphous films [17] have also been investigated.

There is huge gap in the sequential studies of the doped films as well as the in correlation of electrical properties with the structure and morphology of the Sn doped samples. The detailed study of optical parameters like absorption coefficient, refractive index and optical conductivity and their relationship with the obtained structural phase is very important in designing any solar cell configuration. The present study deals with the deposition of the thin films of Sb_2S_3 on the glass substrates by the cost effective chemical bath deposition method at 10 ^oC. The effects of doping of 1% Sn in place of Sb is carried out and the structural, optical and the morphological properties of the doped thin films are discussed. The detailed crystallographic phase analysis and lattice parameters are computed and discussed in relation to the variation in optical properties. Annealing effects on the properties are also discussed.

2. Experimental

Antimony trichloride ($SbCl_3$, Merck, 99%), sodium thiosulphate ($Na_2S_2O_3$, Aldrich, 99%) and acetone (CH_3COCH_3, Merck, 99%) were used as received. The microscopic glass slides were used as substrates. These were cleaned well prior to the deposition. The cleaning was carried out by the hot water, ethyl alcohol, chromic acid and then by the distilled water. These slides were then dried in vacuum for 1hr at 100 ºC. The solution bath was prepared in a 100ml beaker by dissolving 650mg of $SbCl_3$ in 10ml of acetone, then 25ml of 1M $Na_2S_2O_3$ solution with 65ml of distilled water was added and stirred well. The pH of the resulting solution was measured to be 3.5 [18]. The clean microscope glass slides were placed vertically in the bath beaker for a deposition time of 4hrs at 10 ^oC. The deposited films were annealed at 250 ^oC under vacuum for 2 hours. The respective sample codes are given in Table 1.

Structural and optical characterization of the deposited films was carried out using the following equipments. Phase composition and crystallinity of thin films were studied by X-ray diffraction analysis at a 2θ of 20-80º using PANalytical Xpert' Pro (Holland). Scanning electron microscopy was performed using JEOl, JSM-5910 operating at 20kV with different magnification powers. UV/VIS spectra were taken by the Perkin Elmer Lambda 25 spectrophotometer. Diffused reflectance spectra were taken to calculate the band gaps of the deposited thin films using Perkin Elmer Lambda 950 spectrophotometer. Rutherford backscattering spectroscopy was carried out using 5MV pelletron Tandem Accelerator with He^{++} beam having energy of 2.084 MeV.

Table 1: Sample codes for the deposited thin film samples

Sample Codes	Details of the samples
U-1	Un-annealed, Sb_2S_3
U-2	Un-annealed, $Sn_xSb_{2-x}S_3$
A-1	Annealed, Sb_2S_3
A-2	Annealed, $Sn_xSb_{2-x}S_3$

3. Results and Discussion

3.1 Structural properties:

X-ray diffraction analysis was carried out to study the phase development of the deposited thin film samples. Figure 1 shows the comparison of X-ray diffraction patterns of the thin film samples along with the standard Sb_2S_3 pattern (ICSD-06-0474). Well crystalline broad peaks are obtained for the annealed samples.

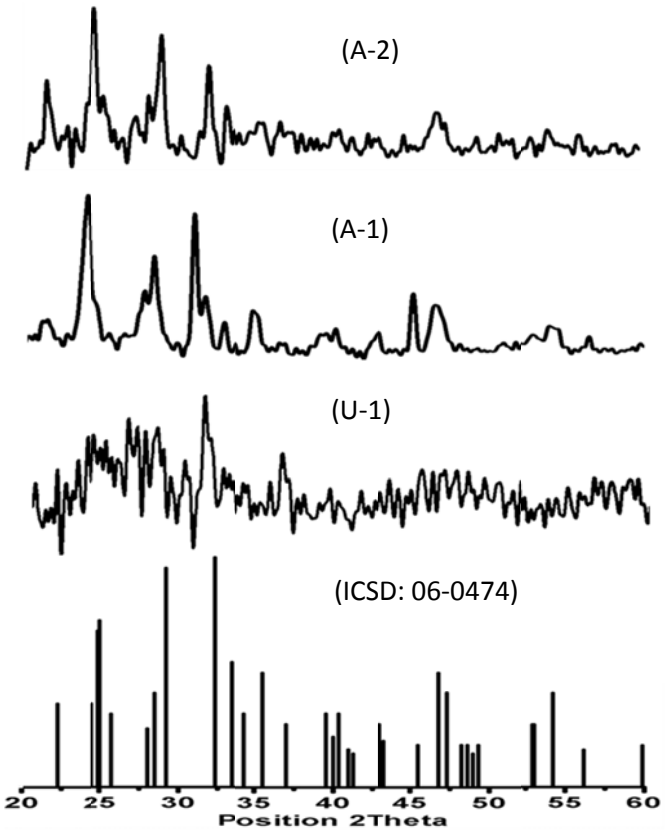

Fig. 1: Comparison of X-ray diffraction patterns of the deposited samples with the standard pattern of Sb_2S_3 (ICSD: 06-0474)

Annealing at 250 ^oC transforms the microcrystalline phase (U-1) to well defined polycrystalline orthorhombic crystal structure (A-1) as shown in Figure 1. The 2theta and d-spacing values of the respective peaks are compared with the standard pattern of Sb_2S_3 in Table 2.

Table 2: A comparison of 2theta and d-spacing values of the deposited thin film samples with the standard pattern of Sb_2S_3, $SnSb_2S_4$ and $Sn_2Sb_2S_5$

ICSD: 06-0474 **Sb_2S_3**		ICSD: 016-0577 $SnSb_2S_4$		ICSD: 034-0620 $Sn_2Sb_2S_5$		U-1		A-1		A-2	
2theta	d-spacing	2theta	d-spacing	2theta	d-spacing	2theta	d-spacing	2theta	d-spacing	2theta	d-spacing
22.28	3.987	**21.82**	**4.070**	23.68	3.750	20.408	4.352	22.44	3.965	**21.92**	**4.055**
24.90	3.573	**23.21**	**3.830**	26.38	3.380	31.668	2.825	-	-	24.95	3.569
25.02	3.556	**27.81**	**3.200**	30.22	2.960	33.042	2.711	25.05	3.556		-
28.53	3.128	**36.97**	**2.420**	30.97	2.890	43.040	2.101			28.48	3.128
29.23	3.053			31.37	2.840	59.895	1.543	29.24	3.058	29.23	3.053
32.36	2.764*			31.97	2.790			31.76	2.817	32.36	2.775
33.41	2.680			39.28	2.290			33.49	2.674	33.34	2.685
35.53	2.525			45.96	1.970			35.38	2.524	**36.87**	**2.518**
40.36	2.233							43.31	2.095	40.40	2.238
46.79	1.940							45.42	1.940	46.89	1.934
52.91	1.729								-	**50.94**	**1.711**
54.21	1.691							54.37	1.686	54.14	1.693

Some of the peaks in the Sn doped sample match with the standard pattern of $SnSb_2S_4$ indicated in bold case in Table 2, while the peak positions of the $Sn_2Sb_2S_5$ are also given for comparison. The peak positions in the U-1 sample do not match with standard Sb_2S_3 sample. The indexing of the patterns was done by comparing with the standard pattern (ICSD-06-0474) and the hkl values are used for the calculation of the lattice parameters. Lattice parameters "a, b and c", unit cell volume "V_{cell}", Scherrer crystallite size "D" and X-ray density "$\rho_{x\text{-}ray}$" are calculated using the following relations for the orthorhombic crystal structure:

$$\frac{1}{d^2} = \frac{h^2}{a^2} + \frac{k^2}{b^2} + \frac{l^2}{c^2} \tag{1}$$

$$V_{cell} = abc \tag{2}$$

$$D = \frac{k\lambda}{\beta \cos\theta_B} \tag{3}$$

$$\rho_{x-ray} = \frac{ZM}{V_{cell} N_A} \tag{4}$$

where d is value of d-spacing of lines in XRD pattern, hkl are corresponding miller indices of each line in the pattern, β is the full width half maximum, λ is the X-ray wavelength (1.542 Å), θ the Bragg's angle and K the constant which is equal to 0.9, Z is the number of molecules per formula unit which is 4 for the orthorhombic structure, M is the molar mass, V_{cell} is the unit cell volume and N_A is the Avogadro's number. The calculated structural parameters of the deposited films are compared with the standard pattern and are given in Table 3.

Table 3: Calculated structural parameters for the deposited thin film samples

Parameters	JCPDS: 06-0474	U-1	A-1	A-2
a (Å)	11.23	11.31	11.47	11.27
b (Å)	11.31	10.51	11.22	11.28
c (Å)	3.84	3.88	3.81	3.83
V_{cell} (Å ^{3})	488	461	490	487
$\rho_{x\text{-}ray}$ (g/cm^3)	4.63	4.88	4.60	4.66
D (nm)	-	15	21	22

The U-1 sample shows the anomalous behavior as its peaks positions are not matched with the standard pattern of Sb_2S_3. A slight increase in lattice parameter 'a' is observed in A-1 sample while the lattice parameters 'b and c' remains constant. This may be attributed to the effective ionic radii of Sb^{3+}, Sn^{4+} and Sn^{2+} which are respectively, 0.62, 0.71 and 1.12 Å. Though, Sn^{2+} is thermodynamically more favorable than Sn^{4+}, the tendency for solid solubility of a solute ion increases as its radius is closer to that of the solvent ion so this evidence supports the presence of Sn^{4+} in the lattice and the cationic vacancies may generate as a result. X-ray density values are comparable to the standard value. The Scherrer crystallite size calculated from equation 4 is 15, 21 and 22 respectively, for the U-1, A-1 and A-2 sample. Chemical composition of the thin film samples has been determined by the RBS spectroscopy and the results are listed in Table 4.

Table 4: Chemical composition (atomic percents) of the elements in the deposited thin films as determined by RBS spectroscopy

Sample	Layers	Thickness (nm)	Sb	S	Sn	Si	O
U-1	Layer 1	144	38.16	61.83	-	-	-
	Layer 2	98	2.03	3.32	-	29.70	61.64
	Layer 3	4000	-	-	-	27.01	70.95
A-1	Layer 1	259	40.60	59.39	-	-	-
	Layer 2	4000	-	-	-	32.61	64.42
A-2	Layer 1	117	39.26	59.76	0.97	-	-
	Layer 2	107	2.27	5.74	0.09	27.66	60.11
	Layer 3	4000	-	-	-	28.68	68.44

The theoretical values for the atomic percent of elements in Sb_2S_3 are (Sb:S = 40:60) while for SiO_2 the theoretical atomic percents are (Si:O = 33.33:66.67). As seen in Table 4, there is no indication of the formation of oxides so the phase of the deposited material is strictly sulphide. Comparing the as deposited and the annealed Sb_2S_3 sample, the atomic percents match the theoretical values within the limits of experimental errors. There seems to be little diffusion of Sb and S into the glass substrate but after annealing no such diffusion is observed. The slight diffusion is also observed in the Sn doped sample. The thickness of the doped film is lowest compared with the other samples as shown in Table 4. Doping by Sn has a remarkable effect on the morphology of the Sb_2S_3 thin films as seen in low and high magnification images of annealed and doped thin film samples shown in Figure 2. The grain growth is enhanced on the account of doping while uncontrolled growth is observed in the undoped thin film samples.

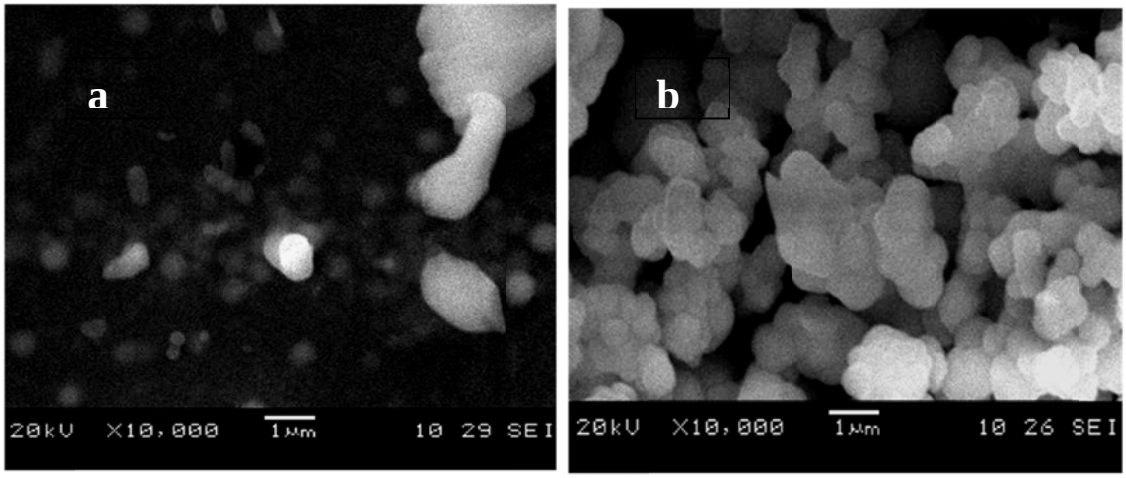

Fig. 2: Enhanced grain growth on the account of Sn doping as seen in the scanning electron micrographs of the deposited samples: a) A-1 and b) A-2

3.2 Optical properties

The Tauc equation is given below which is used to calculate the band gaps of the deposited films:

$$(\alpha h\nu)^n = A(h\nu - E_g) \tag{5}$$

where h is Planks constant, hυ is the energy of electromagnetic radiation, α is the absorption coefficient, E_g is the band gap and A is the proportionality constant. The value of exponent n can be 2, 2/3, 1/2 and 1/3 for the direct allowed, direct forbidden, indirect allowed and indirect forbidden transitions, respectively. The best fit to the experimental data is obtained for n = 2 and the corresponding direct allowed band gaps are given in Table 5. The literature data on the band gap for Sb_2S_3 films is variable and the band gaps are found to be dependent on the crystallinity of the films, atomic/weight ratios of Sb and S and the deposition method **[19]**. The obtained values of the band gap energies (1.50-1.90 eV) indicate the suitability of the deposited films for the solar cell applications.

The variation of absorbance (A) is studied in the wavelength range of 400-800 nm for all the deposited samples. The other parameters which include transmittance (T), reflectance (R), absorption coefficient (α), extinction coefficient (k), refractive index (n), band gap (E_g), dielectric constant (ε), electrical conductivity (σ_e), optical conductivity (σ_o) and the thermal conductivity (σ_t) are calculated using the relations given in [20]: Each parameter has its own significance and doping of Sn has a marked effect on the optical properties. Transmittance and reflectance are calculated from the following relations [20]:

$$T = 10^{-A} \tag{6}$$

$$R = 1 - [T\exp(A)]^{1/2} \tag{7}$$

The plot of absorbance against wavelength is shown in Figure 3. The verification of the band gaps calculated from the Tauc plots is evident from the absorption plots in Figure 3. The absorption edges of the samples are found at almost the same wavelength positions as given by the Tauc plots confirming the direct allowed band gaps in all the deposited samples. The annealing has a marked effect on the absorption properties of the films with a transformation from the narrow band to the broad band absorption in the range of 750-400 nm.

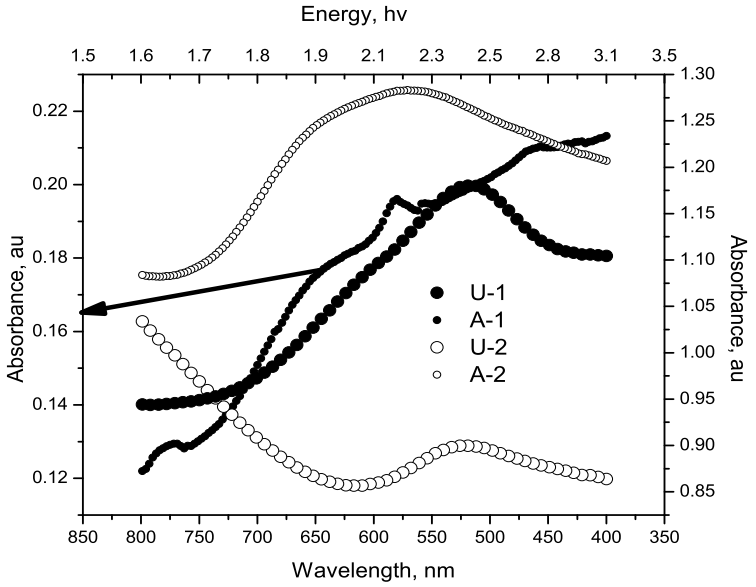

Fig. 3: Plots of absorbance (A) against wavelength (λ) and energy (hv) for the deposited samples.

The absorption coefficient is calculated from reflectance, transmittance and the thickness data of the thin film as given in the relation below:

$$\alpha(cm^{-1}) = \frac{1}{d}\ln\frac{(1-R)^2}{T} \tag{8}$$

The plot of absorption coefficient is shown in Figure 4 and it supports the absorption data in Figure 3. The values of absorption coefficient range from 0.09-1.11 x 10^5 cm^{-1} as shown in Table 5. The highest value being for the annealed Sn doped sample with a broad hump in the range of 450-700 nm. The values of the absorption coefficient obtained in this study are comparatively higher than the values reported in the literature. The high values of absorption coefficient validate their use in photovoltaic applications.

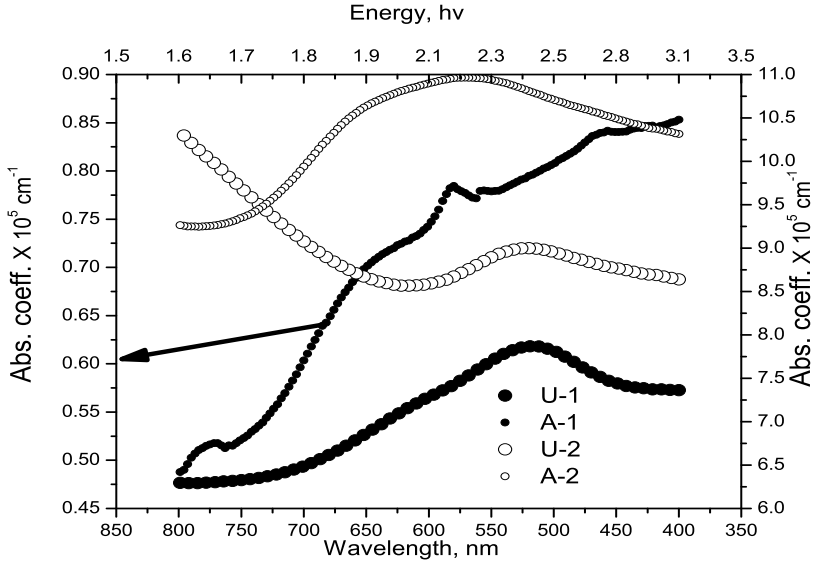

Fig. 4: Absorption coefficient (α) against wavelength (λ) for the deposited samples.

The refractive index is calculated using the following relation:

$$n = \frac{1+R}{1-R} + \sqrt{\frac{4R}{(1+R)^2} - k^2} \tag{9}$$

The refractive index decreases with the wavelength with a broad hump at wavelength of 450-550 nm. The maximum value of refractive index is 4.20 at 417 nm. The annealing has a marked effect on the refractive index as it decreases to a value below 3.8. The refractive index of the doped sample shows a similar behavior but it is highest for the annealed sample and stays in the range of 3.9-4.5 with a maximum value at 500-600 nm.

Table 5. Optical parameters of the deposited samples calculated from UV/VIS absorbance data

Sample codes	α x10^5 (cm^{-1})	E_g (eV)	n	ε	σ_e $(\Omega.cm)^{-1}$	σ_o x10^{14} (s^{-1})	σ_t x10^{-4} (W/m.K)
U-1	0.78	1.54 (805 nm)	4.20	20	1.29	4.74	9.4
A-1	0.09	1.50 (827 nm)	1.93	4	2.70	0.39	19.7
U-2	0.90	1.90 (653 nm)	3.47	17	1.52	2.82	11.0
A-2	1.11	1.58 (785 nm)	4.40	23	1.20	5.31	8.80

The maximum value of dielectric constant is 20 observed at 525 nm and is calculated using the relations below. The annealing lowers the dielectric constant values. The doping by Sn has an effect on the pattern of dielectric values with the highest values for the annealed sample.

$$\varepsilon = (n - ik)^2 \tag{10}$$

The electrical conductivity is calculated from refractive index data as given in equation 11.

$$\sigma_e(\Omega cm)^{-1} = \frac{2\pi}{\lambda nc} \tag{11}$$

The electrical conductivity increases as the absorption edge is surpassed at ~ 830-650 nm. The electrical conductivity is lower for the annealed Sn doped sample.

The thermal conductivity of the deposited samples is calculated using the following relation:

$$\sigma_t(W/mK) = LT\sigma_e \tag{12}$$

where L is the Lorentz number (2.45x10^{-8} WΩK^{-2}), T is temperature and σ_e is the electrical conductivity. The thermal conductivity of the annealed Sn doped sample is lowest while for the unannealed Sn doped sample, its value is highest. The maximum value of thermal conductivity for each sample is given in Table 5. The optical conductivity is calculated from the following relation:

$$\sigma_o(s^{-1}) = \frac{\alpha nc}{4\pi} \tag{13}$$

The optical conductivity of the annealed Sn doped sample is highest showing a maximum in the range of 500-650 nm wavelength.

4. Conclusion

Thin films of Sb_2S_3 have been successfully deposited by the chemical bath deposition method. The effects of doping of 1% Sn in place of Sb is carried out and the structural, optical and the morphological properties of the doped thin films are discussed. Annealing at 250 ^oC transforms the microcrystalline phase to well defined polycrystalline orthorhombic crystal structure and supports the presence of Sn^{4+} in the lattice and the cationic vacancies may generate as a result. The atomic percents match the theoretical values within the limits of experimental errors. The obtained values of the band gap energies (1.50-1.90 eV) and high values of absorption coefficient ~ 10^5 cm^{-1} indicate the suitability of the deposited films for the solar cell applications.

References

[1] E. Serrano, G. Rus, J.G. Martinez, Renew. Sustainable Energy Rev. **13**, 2373 (2009).
[2] V. Devabhaktuni, M. Alam, S. Shekara, S.R. Depuru, R.C. Green, D. Nims, C. Near, Renew. Sustainable Energy Rev. **19**, 555 (2013).
[3] B. Parida, S. Iniyan, R. Goic, Renew. Sustainable Energy Rev. **15**, 1625 (2011).
[4] M.Y. Versavel, J.A. Haber, Thin Solid Films **515**, 5767 (2007).
[5] C. Li, G. Shi, Y. Song, X. Zhang, S. Guang, H. Xu, J. Phys. Chem. Solids **69**, 1829 (2008).
[7] S. Srikanth, N. Suriyanarayanan, S. Prabahar, V. Balasubramanian, D. Kathirvel, Adv. Appl. Sci. Res. **2**, 95 (2011).
[8] K.F. Abd-El-Rahman, A.A.A. Darwish, Curr. Appl. Phys. **11**, 1265 (2011).
[9] F.I. Ezema, S.C. Ezugwu, P.U. Asogwa, A.B.C. Ekwealor, J. Ovonic Res. **5**, 145 (2009).
[10] S.M. Salim, M.B. Seddek, A.M. Salem, Islam, J. Appl. Sci. Res. **6**, 1352 (2010).

[11] E. Cardenas, A. Arato, E.P. Tijerina, T.K. DasRoy, G.A. Castillo, B. Krishnan, Solar Energy Mater. Solar Cells **93**, 33 (2009).
[12] C. Garza, S. Shaji, A. Arato, E.P. Tijerina, G.A. Castillo, T.K. DasRoy, B. Krishnan, Solar Energy Mater. Solar Cells **95**, 2001 (2011).
[13] F. Perales, F. Agull´o-Rueda, J. Lamela, C. de las Heras, J. Phys. D: Appl. Phys. **41**, 045403 (2008).
[14] B. Frumarova, M. Bılkova, M. Frumara, M. Repka, J. Jedelsk, J. Non-Cryst. Solids **326-327**, 348 (2003).
[15] D. Topa, E. Makovicky, The Canadian Mineralogist, **48**, 1119 (2010).
[16] A. Gassoumi, M. Kanzaria, B. Rezig, Eur. Phys. J. Appl. Phys. **41**, 91 (2008).
[17] A. Gassoumi, M. Kanzaria, Chalcogenide Lett. **6**, 163 (2009).
[18] F. Aousgi, M. Kanzari, Energy Procedia **10**, 313 (2011).
[19] A.M. Salem, M.S. Selim, J. Phys. D: Appl. Phys. **34**, 12 (2001).
[20] C.D. Lokhande, B.R. Sankapal, R.S. Mane, H.M. Pathan, M. Muller, M. Giersig, V. Ganesan, Appl. Surf. Sci. **193**, 1 (2002).
[21] P.A. Ilenikhena, Afr. Phys. Rev. **2**, 0008 (2008).